Structural and spectroscopic analysis of *ex-situ* annealed RF sputtered aluminium doped zinc oxide thin films

Francis Otieno, Mildred Airo, Rudolph M. Erasmus, et al.

View Online   Export Citation   CrossMark

ARTICLES YOU MAY BE INTERESTED IN

CrossMark
click for updates

Structural and spectroscopic analysis of *ex-situ* annealed RF sputtered aluminium doped zinc oxide thin films

Francis Otieno,[1,2,3] Mildred Airo,[4] Rudolph M. Erasmus,[1,2] David G. Billing,[2,4] Alexander Quandt,[1,2,3] and Daniel Wamwangi[1,2,3]

[1]*Material Physics Research Institute, School of Physics, University of the Witwatersrand, Private Bag 3, Wits 2050, Johannesburg, South Africa*
[2]*Materials for Energy Research Group, University of the Witwatersrand, Private Bag 3, Wits 2050, Johannesburg, South Africa*
[3]*Museo Storico della Fisica e Centro Studi e Ricerche Enrico Fermi, Piazza del Viminale 1, 00184 Roma, Italy*
[4]*School of Chemistry, University of the Witwatersrand, Private Bag 3, Wits 2050, Republic of South Africa*

Aluminium doped zinc oxide thin films are prepared by Radio Frequency magnetron sputtering in pure argon atmosphere at 100 W. The structural results reveal good film adhesion on a silicon substrate (001). The thin films were then subjected to heat treatment in a furnace under ambient air. The structural, morphological, and optical properties of the thin films as a function of deposition time and annealing temperatures have been investigated using Grazing incidence X-Ray Diffraction (GIXRD), Atomic Force Microscopy, and Scanning Electronic Microscopy. The photoluminescence properties of the annealed films showed significant changes in the optical properties attributed to mid gap defects. Annealing increases the crystallite size and the roughness of the film. The crystallinity of the films also improved as evident from the Raman and XRD studies. *Published by AIP Publishing.* [http://dx.doi.org/10.1063/1.4998939]

I. INTRODUCTION

Environmental friendly ZnO has received much attention over the past decades as a result of its wide and direct band gap (3.27 eV) as well as the large exciton binding energy (60 meV).[1] Through band gap engineering such as alloying with MgO or CdO, its properties can be extended to numerous applications. This makes it a good candidate for various applications such as gas sensors and transparent conductors for optoelectronic applications. Other important characteristics of ZnO include: strong luminescence in the green-white region of the spectrum making it a suitable material for phosphor application and as a base material for up and down-conversion;[2] availability of large area single crystals and epi-ready substrates hence make it easy to grow thin films using diverse methods such as chemical vapor deposition, molecular beam epitaxy, laser ablation or sputtering.[3–5] ZnO crystallizes in the thermodynamically stable wurtzite structure almost always as an n-type wide band gap semiconductor, the cause of which has been a matter of intensive debate.[6] The low symmetry of the wurtzite crystal structure combined with the large electromechanical coupling in ZnO also gives rise to strong piezoelectric and pyroelectric properties.[7,8] Various research groups have reported that the opto-electrical properties of ZnO can be significantly changed using a relatively small concentration of native point defects and impurities (transition metals and rare earths).[9,10]

Recently, aluminium doped ZnO has shown high potential as a low cost alternative to indium tin oxide (ITO) commonly used as a transparent conducting electrode in solar cells and light emitting diodes (LED's). This is also as a result of its abundance in nature and its non-toxicity as well as its non-electrode poisoning capability. It also exhibits good electrical conductivity, high optical transparency within the visible region (400–800 nm), as well as good mechanical, chemical, and thermal stability ($T_m = 2248K$).[11]

Among the various growth techniques for Al doped ZnO, Radio Frequency (RF) magnetron sputtering has its advantages such as ability to produce good quality films with a high surface area and low electrical resistivity. This deposition can be carried out at room temperature yet exhibit high stability at elevated temperatures.[1]

In the present study, the effect of deposition time and post-growth annealing of RF sputtered Al doped ZnO thin film at a temperature range of 600–1000 °C in air are investigated. High temperature annealing appears to enhance green-white photoluminescence (PL) intensity, improve crystallinity, as well provide a mechanism for the substitution of zinc doping in the presence of Al impurity. A high crystallinity is essential to reduce the phonon velocities thereby limiting the probability of non-radiative transitions which quench the emission intensity of rare earths used for up and down conversion applications.

II. EXPERIMENTAL DETAILS

Aluminium doped ZnO thin films have been deposited using RF magnetron sputtering onto n-type (001) Silicon substrates at room temperature. The substrates were initially cleaned with acetone and ethanol in an ultrasonic bath for 20 min and rinsed in deionized water before drying using a stream of nitrogen gas. The substrates were then mounted on a rotating substrate holder at a distance of 6 cm from the ZnO target. The target used was ZnO (98%): Al (2%) disk (99.99% purity) with a diameter of 76 mm and thickness 6 mm. This was bonded onto a circuit magnetron cathode in

a vertical configuration. The sputtering chamber was evacuated to a base pressure of about 2×10^{-5} mbar while sputtering was performed under Argon with a working gas pressure of 2.3×10^{-3} mbar. The growth was undertaken under 13-sccm Ar flow, 100 W RF power with deposition time varied between 5 and 60 min. Post-growth annealing was carried out in air for films deposited for 40 min in a furnace at a temperature range of 600–1000 °C for 2 h.

A. Characterization of the films

The morphologies and structural analyses of the samples were characterized using Veeco Di-3100 atomic force microscopy (AFM) in tapping mode and FEI Nova Nanolab 600 scanning electronic microscopy (SEM). The elemental composition of the films was analysed using an energy dispersive X-ray diffractometer spectroscopy (EDX) attached to the SEM. The Raman bands and the structural order of all the films were examined using a Horiba LabRAM HR Raman spectrometer equipped with an Ar ion laser (514.5 nm) and a laser power of <1 mW at the sample. The effect of deposition time and post growth annealing temperature on the crystallinity and phase were studied using an AXS Bruker D8 Discover, 40 kV, 40 mA using CuKα radiation in the Seeman–Bohlin geometry. The scanning range of 2θ was varied from 10° to 80° at a low scanning rate of 1.2 deg/min. The X-ray reflectivity (XRR) and diffraction spectrum of the sample were recorded before XRR curve fitting using the Diffrac-Leptos software. Photoluminescence measurements were carried out using a Horiba LabRAM HR spectrometer with a 150 lines/mm grating

and an excitation wavelength of 229 nm from a frequency doubled Lexel argon ion laser.

III. RESULTS AND DISCUSSION

A. Morphology studies by AFM and SEM

The surface morphology of the ZnO:Al films was characterized using the Veeco Di3100 AFM under the tapping mode and the results are shown in Fig. 1.

The surface topographic parameters such as the average roughness (R_a), root mean square roughness (R_{rms}), skewness (R_{sk}), and kurtosis (R_{ku}) parameters are summarized in Table II.

From Table I, the average roughness of the film surface increases with annealing temperature showing that the degree of uniformity of the surface decreases with increases in temperature. Indeed, the surface reconstruction as a result of formation of native defects can vary over a wide range (given by the formation enthalpy of ZnO, i.e., 3.6 eV) as a function of the chemical potentials.[7]

We further tabulated the skewness (R_{sk}) and the kurtosis (R_{ku}) which give a measure of the asymmetry and the sharpness, respectively. The skewness (R_{sk}) was used to establish the profile symmetry about the mean line. The positive values of the skewness parameter indicate that the height distribution is asymmetrical with more peaks than valleys.[11] Annealing enhances surface diffusion and oxidation leading to shape and size reconstruction and hence an increasing trend of the skewness. Kurtosis (R_{ku}) on the other hand gives the measure of surface sharpness of the film surface. Since
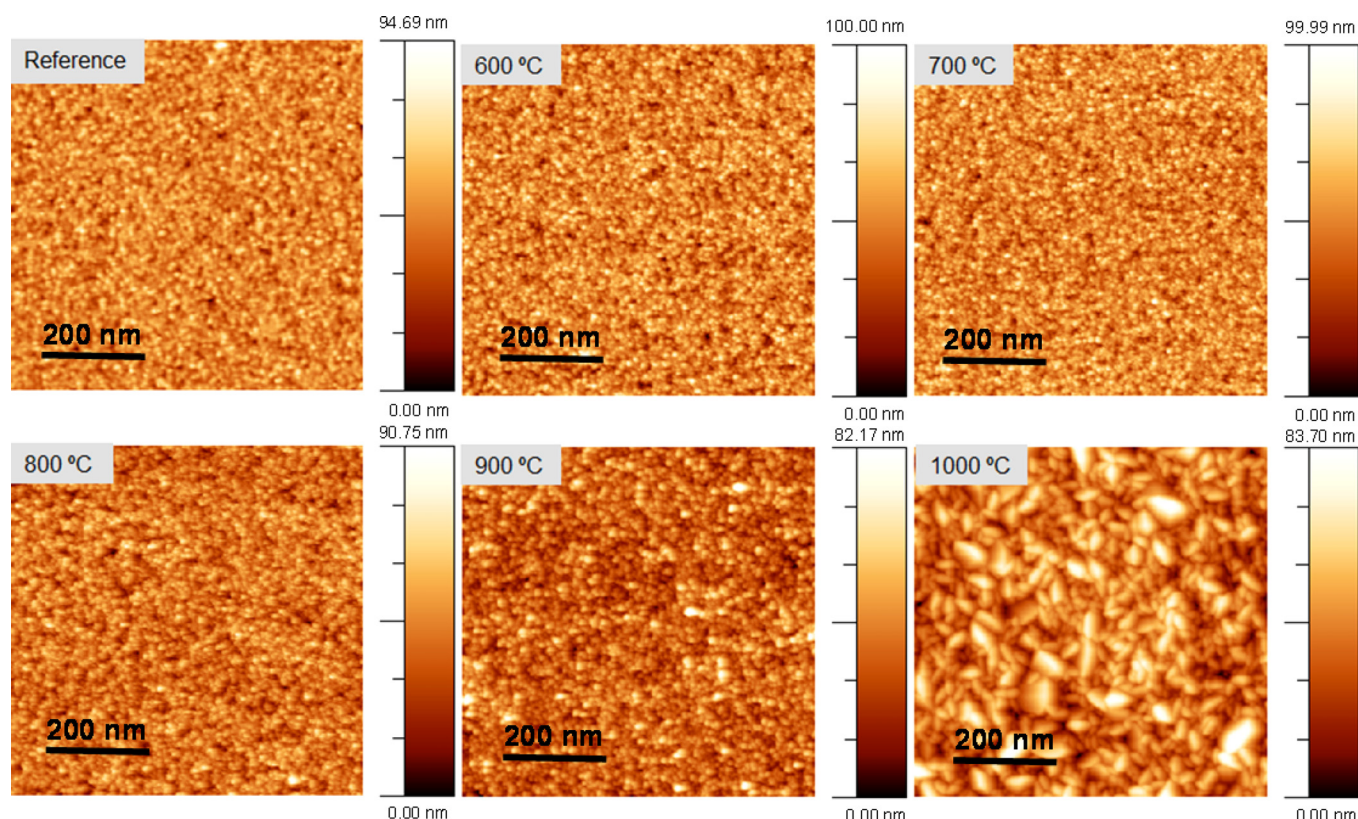

FIG. 1. AFM images of the Al doped ZnO films grown at constant deposition time before and after annealing at a temperature range of 600–1000 °C in air.

TABLE I. Summary of tapping mode AFM analysis of films annealed at different temperatures.

Annealing temperature (°C)	R_a (nm)	R_{rms} (nm)	Skewness (R_{sk})	Kurtosis (R_{ku})	Grain height (nm)
Reference	3.43	4.317	0.002	3.162	8.06
600	4.567	5.747	0.016	3.076	22.56
700	4.310	5.414	0.087	3.045	22.683
800	4.608	5.775	0.042	3.035	21.065
900	5.777	7.428	0.654	4.222	27.244
1000	28.563	35.883	0.653	4.132	94.149

the kurtosis (R_{ku}) is higher than 3, the surface has more peaks than valleys.

The grain height is observed to increase with temperature. This is attributed to the process of coalescence and surface oxidation. This is consistent with the grazing incidence x-ray diffraction (GIXRD) results; however, the values are seemingly larger than those obtained from XRD analysis due to the fact that AFM gives the particle size while XRD derives the grain size.

When annealed at high temperatures, the atoms acquire enough energy to overcome the activation energy of self-diffusion and thus occupy lattice site in the crystal. Grains of Bragg reflexes 100, 002, and 112 with the lower surface energy will become larger.[12] At 1000 °C, there is a sharp increase in both roughness and grain height due to grain growth. On the account of vacancy reduction, larger grains are formed in a process similar to sintering. Zinc has a greater volume diffusion than oxygen.[13] Zn self-diffusion may be mediated by Zn vacancies which have a higher migration

barrier of 1.40 eV, but with much lower formation energy in n-type ZnO.[14] Indeed, Tomlins *et al.* reported an activation energy of Zn in ZnO of 3.86 eV for self-diffusion compared to Oxygen in ZnO, and appropriately suggested that Zn self-diffusion is controlled by a vacancy mechanism.[7]

Figure 2 shows the AFM image of films deposited at an RF power of 100 W at varied deposition time. At low deposition time flat islands, often with highly dendritic shapes are formed following the Volmer–Weber growth mode. An increase in deposition time leads to the formation of "spherical" like thicker films. This is confirmed by the increase in grain height with time as well as film thickness increase measured using the thickness profilometer. From Table II, the roughness first increases with deposition time as larger porous particles are formed. At 40 min deposition time, the film appears more compact with a reduced roughness. This is also observed at a deposition time of 1 h.

The SEM micrographs of Al doped ZnO grown at an RF power of 100 W for 40 min shows that the films exhibit a smoother and uniform texture upon growth. The particles assume an almost spherical shape indicating a homogenous nucleation process involved in the RF sputtering (Fig. 3). The emergence of small crack in the as-grown film is a clear indication of competition between strain and film-substrate adhesion in the as-deposited films. With the increase of the annealing temperature, the strain relaxation occurs as the smaller strained grains are aggregated into larger grain sizes which are less strained.[15] This is corroborated from the change in lattice parameters and c/a ratio. A comprehensive discussion is presented in Sec. III C. At 1000 °C, the surface is smooth but with huge gaps between the blocks resulting
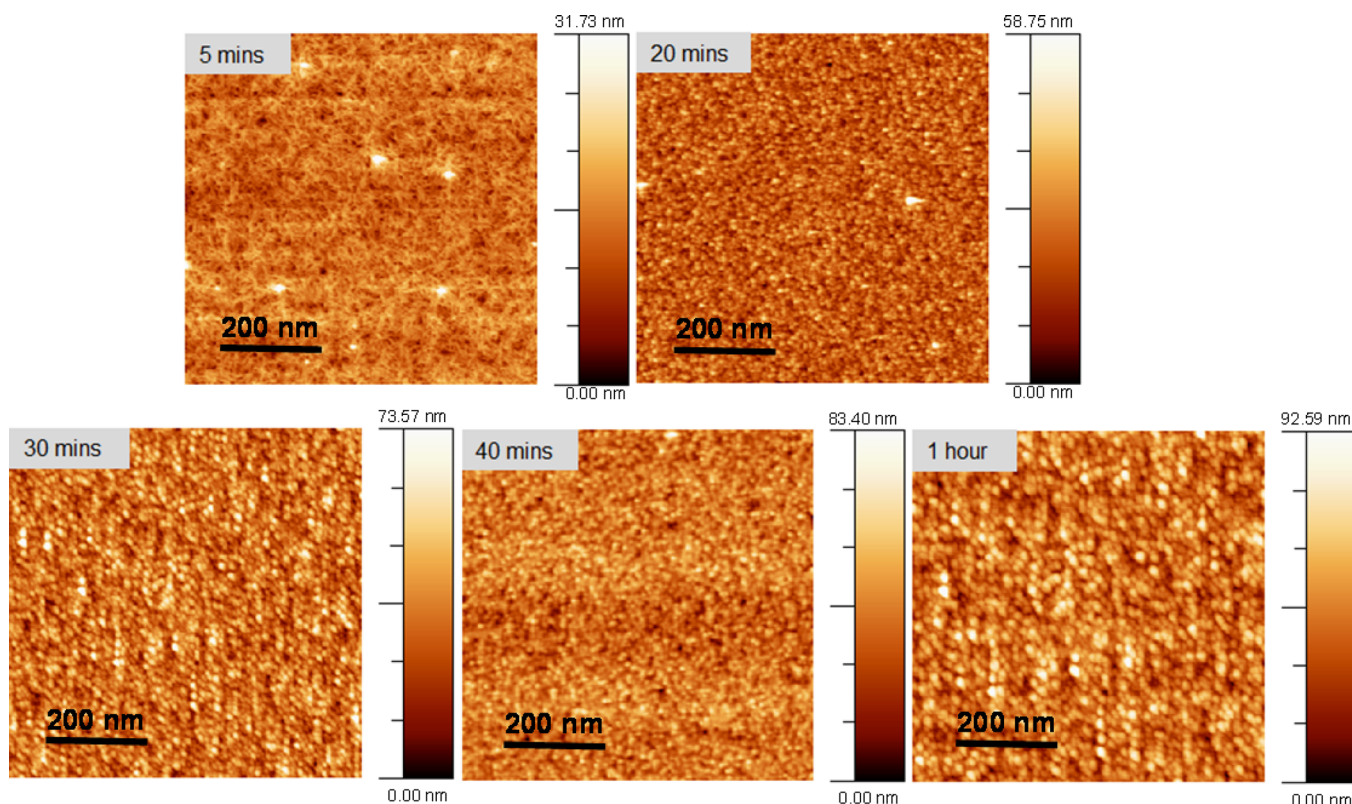

FIG. 2. AFM images of the Al doped ZnO grown at an RF power of 100 W over different deposition times ranging from 5 min to 1 h at room temperature.

TABLE II. Summary of tapping mode AFM analysis.

Deposition time (min)	Film thickness (nm)	R_a (nm)	R_{rms} (nm)	Skewness (R_{sk})	Kurtosis (R_{ku})	Grain height (nm)
5	138	2.25	3.19	3.233	53.86	8.06
20	379	2.63	3.29	0.289	3.74	10.18
30	545	4.12	5.22	0.327	5.031	38.82
40	715	3.43	4.32	0.302	3.162	46.64
60	1048	3.31	4.16	0.244	3.192	53.34

from thermal stress due to mismatch of thermal expansion between the Al doped ZnO and the silicon substrate. For instance ZnO has a thermal expansion coefficient of $4.75 \times 10^{-6} K^{-1}$ while the silicon substrate has a mean thermal expansion of $2.69 \times 10^{-6} K^{-1}$ at room temperature.[16,17] A mismatch in thermal expansion and anisotropic contraction during annealing induces tensile stress on the ZnO film as the substrate cools from high temperature to room temperature and such stress relaxations lead to cracking of films.[18] The EDS spectrum measurement (Fig. 4) shows that there is no impurity from other materials besides Si used as a substrate.

B. Raman spectroscopy

Raman spectroscopy is the inelastic scattering of photons by phonons. This technique is predominantly used for estimating the crystallinity of materials. The finite optical phonons within the grains of ZnO nanostructures result in an interesting change in their vibrational spectra compared to that of their bulk counterparts. Some shifting of peaks as well as broadenings in the Raman spectra may occur for crystals with reduced dimensionality. The Raman spectra of ZnO nanostructures always exhibit such shift and broadening from the bulk phonon frequencies. According to Khan *et al.*, the phonon peak shifts in the Raman spectra of nanostructures is attributed to spatial confinement within the quantum dot nanocrystal boundaries as well as phonon

localization by defects.[19] ZnO is a semiconductor with a wurtzite crystal structure. The wurtzite structure of the ZnO crystal has a C6v symmetry with 4 atoms in the hexagonal unit cell leading to 12 phonon branches, 9 optical, and 3 acoustic, classified according to the following irreducible representations:

$$\Gamma = 2A_1 + 2B_1 + 2E_1 + 2E_2, \tag{1}$$

where A and B modes have one-fold degeneracy and E modes are two-fold. One A_1 mode and one E_1 pair are the acoustic phonons. The 9 optical phonons are divided into one A_1 branch (Raman and IR active), one doubly degenerate E_1 branch (Raman and IR active), two doubly degenerate E_2 branches (Raman active only), and two inactive B_1 branches.[20] The non-polar E2 modes have two wave numbers, namely, E2 (high) and E2 (low) associated with the motion of oxygen and Zn sub lattice, respectively.[19]

Figure 5 shows the various Raman modes obtained using the green excitation wavelength (514 nm, 2.41 eV) in the $100–800 \, cm^{-1}$ range. Raman peaks are observed at 278, 305, 437, 584, and $619 \, cm^{-1}$ in the as-synthesized sample.

The peak intensity at $278 \, cm^{-1}$ gradually reduces with annealing temperature and finally disappears at 800 °C. This peak is attributed to the Raman inactive B_2 mode resulting from the presence of a built-in electric field within the separate grains that lowers the lattice symmetry.[11] As a result of increase in the A_1 (LO) vibrations, another peak due to the existence of a built-in electric field in the crystallites is seen at $584 \, cm^{-1}$. The grain boundaries typically contain a relatively high interfacial density that captures the free carriers from most of the grains. Interface charge gives rise to band-bending in the bulk of the grain and an interface barrier develops. This confirms the substitution of Al in the ZnO. The depletion layer is located near the grain boundary due to the high carrier concentration resulting from Al doping, and the bulk density of the carrier density in most grains is constant. Lowering of the doping level, for example by addition
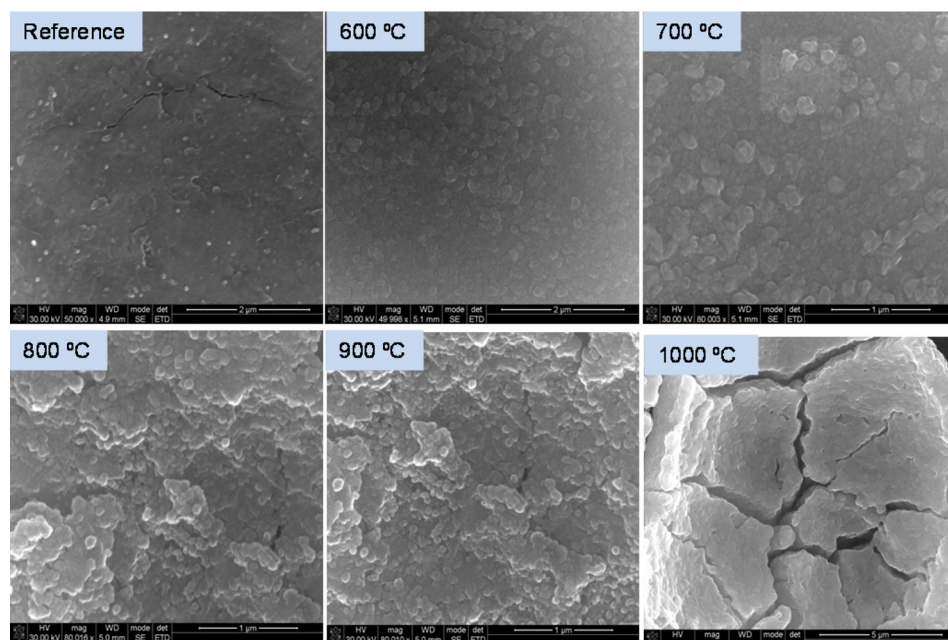

FIG. 3. SEM images of the Al doped ZnO before and after annealing at the temperature range of 600–1000 °C in air.
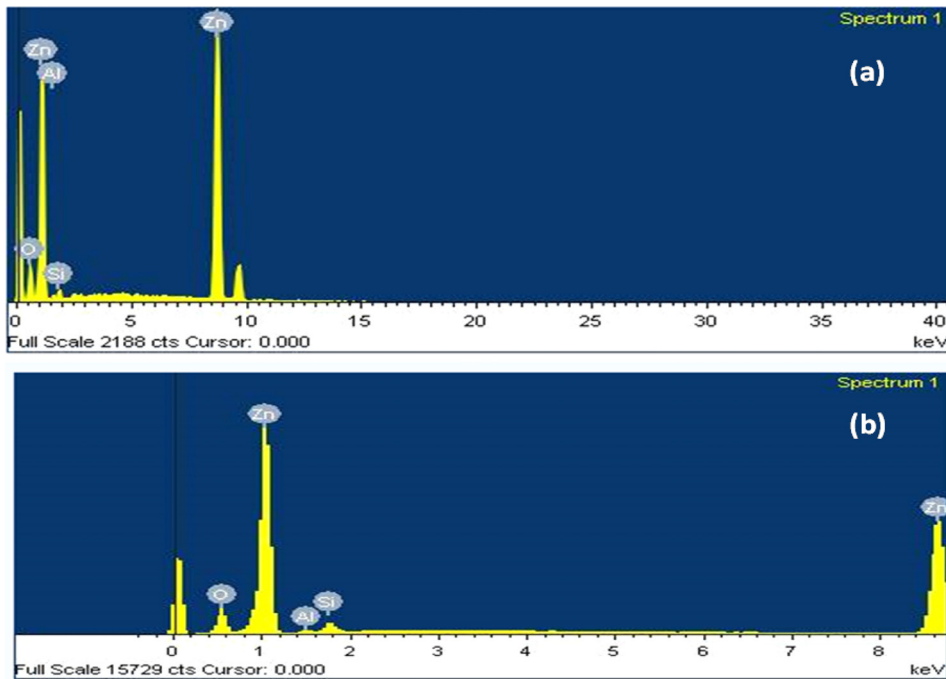
FIG. 4. Energy Dispersive Spectroscopy (EDS) spectra of the (a) pristine and (b) annealed ZnO thin film (1000 °C).

of oxygen during the annealing process, leads to nearly flat bands throughout each grain. This is evident by the peak at 278 cm^{-1} and in the high Raman shift regime, at 584 cm^{-1} which suddenly disappear at annealing temperature of 800 °C. At this temperature, there is formation of more insulating films and hence the value of the built-in electric field decreases and disappears.[21]

A notable peak observed at 437 cm^{-1} in all samples is the assigned E$_2$ (high) mode. Usually, this is the strongest mode in the wurtzite crystal structure and is as a result of oxygen atom motion in the ZnO lattice.[22] The position of the E$_2$ (high) mode shows no obvious change with increasing annealing temperature. The intense peaks at 305 and 525 cm^{-1} are associated with the silicon substrate. However its intensity increases with annealing temperature, an indication of the improving crystalline quality of the films with annealing.[23]

When the time of deposition is varied, the Raman peaks obtained are as shown in Fig. 6.

Figure 6 shows the Raman spectra of the prepared Al doped ZnO thin films with varied deposition times. The Raman lines around 278 cm^{-1}, 437 cm^{-1}, and 584 cm^{-1} were observed for all the samples. These lines are assigned to the ZnO B$_2$ mode, E$_2$ (high) and the A$_1$ longitudinal optical (LO) mode, respectively. The blue shift of the B$_2$ mode peak from 274.1 cm^{-1} to 277.6 cm^{-1} was caused by the tensile strain in the films which was in good agreement with the GIXRD results. The peaks at 278 cm^{-1} and 584 cm^{-1} become intense with narrow FWHM as deposition time increases. This could be attributed to more scatter volume and thermalisation of the substrate for long deposition times as well as an increasing order in ZnO along the basal plane due to the prolonged thermal history of the film for longer deposition times (Fig. 7). The A1 (LO) mode was caused by the defects of O-vacancy and Zn interstitial. The increase of the B$_2$ and A$_1$ (LO) mode intensity for the Al doped ZnO
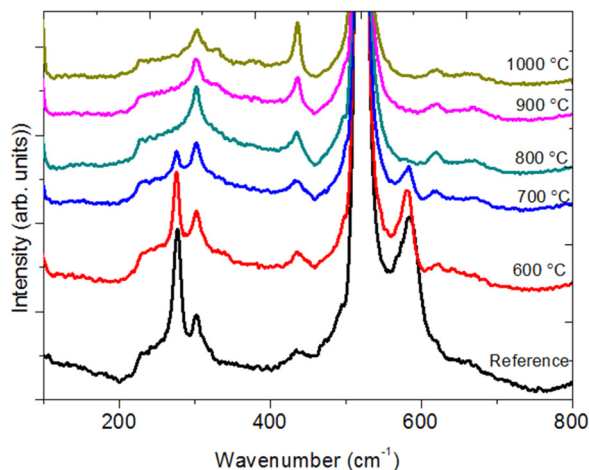

FIG. 5. Raman spectra of the aluminium doped ZnO thin film before and after annealing at 600–1000 °C. The spectra were collected at normal incidence (at 90 °C to the surface normal).
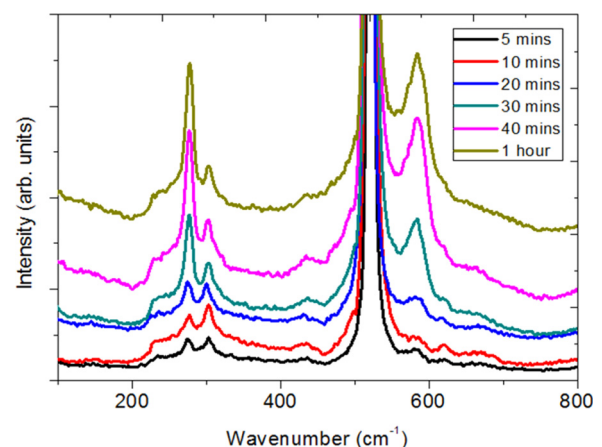

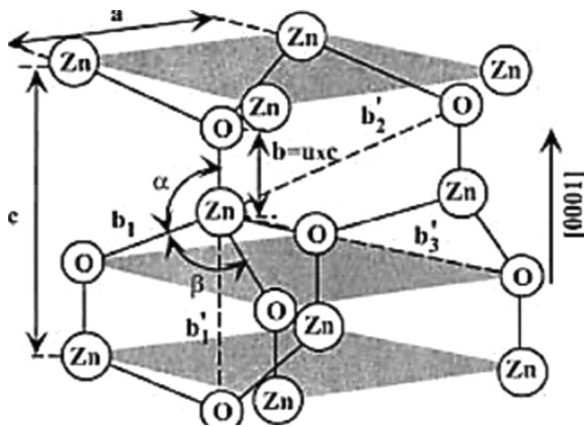FIG. 6. Raman spectra of the Al doped ZnO thin film deposited at 100 W power at different deposition times.

FIG. 7. Schematic representation of a wurtzitic ZnO structure having lattice constants a in the basal plane and c in the basal direction; the u parameter is expressed as the bond length.[25]

thin film with increasing deposition time implied the increase of defects (O- vacancy and Zn interstitial) in this film which is consistent with the PL result.[24]

C. XRD and XRR measurements

The GIXRD patterns of the Al doped zinc oxide films annealed at different temperatures appear in Fig. 8. All the peaks are indexed to the JCP2 card number 003–0888 with a hexagonal wurtzite structure of the space group of P63mc and lattice constants, a = 5.21 Å and c = 3.24 Å. A schematic diagram of the ZnO wurtzite structure is shown in Fig. 6. The structure consists of two interpenetrating hexagonal-close-packed hcp sub lattices. Each sublattice consists of one type of atom displaced with respect to each other along the threefold c-axis by the amount of u = 0.379 defined as the length of the bond parallel to the c axis, in units of c and is given by the following equation:[25]

$$u = \frac{1}{3}\left(\frac{a^2}{c^2}\right) + \frac{1}{4}. \tag{2}$$

From the XRD patterns, the as deposited films are polycrystalline in nature with a preferred orientation along the c-axis. Three distinct peaks (100), (002), and (112) are observed. The (100) and (002) peak intensity increases with increasing

annealing temperature up to 900 °C. The increase in peak intensity is coupled to a reduction in the full wavelength at half maxima (FWHM) indicating enhanced crystallinity (grain growth) in the films with increasing annealing temperature. The increase in peak intensity with annealing temperature between 600 and 900 °C may be attributed to the thermal activation energy acquired by atoms to enhance their mobility in ZnO. The diffusion of oxygen atoms could decrease the vacancy defects in the ZnO films hence improving the quality of films.[12] Beyond 900 °C, the intensity sharply decreases and this may be a result of the presence of porosity.[26]

In ZnO, the most intense peak is usually along the (002) plane, however, this is contrary to our observation in which a higher intensity peak corresponding to the (100) plane is reported. This anomaly is attributed to the disturbance of the charge neutrality induced by Al^{3+} substitution of Zn^{2+}.[27] Furthermore, the presence of Al changes the diffusion rate of Zn and O on the Si substrate during deposition and annealing. This may alter the energetic balance between (100) and (002) orientations hence making the usually preferred (002) orientation in the wurtzite structure[28] to be unfavourable. This peak intensity increases with temperature as a result of more substitution.

At temperatures between 600 and 900 °C, the FWHM of the peaks decreases relative to the strong increase of their intensities (Table III). This observation can be explained using the Scherrer's theory that the full width of a peak at half maximum in a polycrystalline sample is correlated with the extension d of the crystalline domains.[29] The peak positions are shifted to lower wavelength in this temperature regime as a result of compressive stress induced by annealing effects. This may also be due to the fact that more Al ions occupy the lattice position of Zn ions and less stress remains in films after annealing.[30] At 900 °C, the shift in peak position is towards that of the pristine film. Annealing also reduces the concentration of structural defects/pinhole and thus decreases the intrinsic stress. During annealing, atoms of ZnO films acquire energy to arrange leading to reduction in the tensile stress. There are higher chances of Zn self-diffusion mediated by Zn vacancies which have a higher migration barrier of 1.40 eV, but with a much lower formation energy. Indeed, Tomlins *et al.* reported an activation energy

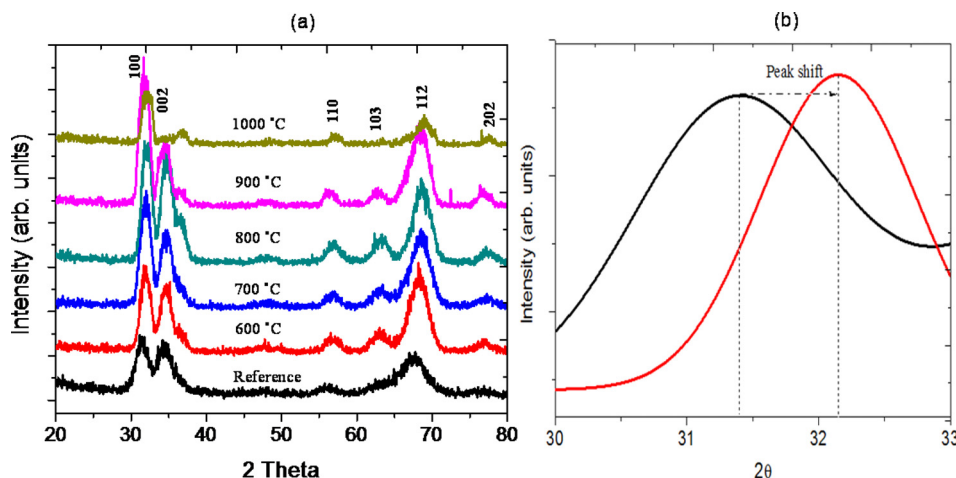FIG. 8. X-ray diffraction (XRD) pattern of (a) the Al doped ZnO thin film before and after annealing at temperature between 600 and 1000 °C in air and (b) curve fit of the (100) peak before and after annealing at 1000 °C.

TABLE III. Characteristics of Al doped ZnO estimated from XRD patterns.

Annealing temperature (°C)	fwhm (100)	2θ (deg)	fwhm (002)	2θ (deg)	fwhm (112)	2θ (deg)
Reference	1.53822	31.3593	2.45638	34.4687	3.54359	67.3477
600	1.32936	31.9170	1.79432	34.7805	2.64725	68.4060
700	1.29202	31.9153	1.73682	34.7051	2.45601	68.2038
800	1.17732	32.0276	1.42188	34.9395	2.26733	68.6342
900	1.28508	31.7629	1.52375	34.4886	2.40098	68.2992
1000	1.19040	32.1506	1.29611	36.6505	1.91422	68.9132

of 3.86 eV for self-diffusion of Zn in ZnO, and appropriately suggested that Zn self-diffusion is controlled by a vacancy mechanism.[8] However, ZnO has a higher thermal expansion coefficient compared to the substrate (Si). Hence, a compressive stress will be generated by Si when the substrate cools to room temperature. This difference causes the shift in the peak position[12] and a decrease in the elastic strain.

The associated stress and strain are evident in the changing lattice constants a and c values as shown in Table IV below.

From the multi-peak fitting carried out using the Origin8 software (originLab corporation), the peak center positions were obtained as recorded in Table III and used to derive the lattice spacing for all the samples using Bragg's relation:

$$\lambda = 2 d_{hkl} \operatorname{Sin} \theta_{hkl}, \tag{3}$$

where θ is the Bragg's angle (angle between normal to the diffracting plane and incident X-ray), λ is the X-ray wavelength which in our case was CuKα radiation with a wavelength of 1.541 Å. The lattice parameters a and c were obtained for the three major peaks using the expression for the hexagonal system[22]

$$\frac{1}{d^2} = \frac{4}{3} \left(\frac{h^2 + hk + l^2}{a^2} \right) + \frac{l^2}{c^2}. \tag{4}$$

The lattice parameters a and c calculated at different annealing temperatures as well as the reference film are nearly equal to the lattice constants given in the standard data (JCP2 card number 003-0888). The slight increase in the lattice parameters with increasing annealing temperature is attributed to the strain in the lattice or stresses induced by the Al dopant which have higher valence states than Zn.

TABLE IV. Estimated crystallite size, lattice parameters, dislocation density, and strain from XRD data.

Annealing temperature (°C)	Crystallite size, D_{sh}/(nm)							
	(100) peak	(002) peak	(112) peak	Average size	a/(Å)	c/(Å)	δ (10^{15})	ε (10^{-3})
Reference	10.73	6.79	5.39	7.63	3.29	5.20	8.69	3.23
600	12.43	9.28	7.26	9.65	3.24	5.16	6.47	2.79
700	12.79	9.58	7.81	10.06	3.24	5.17	6.11	2.71
800	14.04	9.51	8.48	10.67	3.23	5.13	6.07	2.70
900	12.86	12.04	7.99	10.96	3.25	5.19	6.05	2.69
1000	13.89	12.92	10.06	12.29	3.21	4.90	5.18	2.49

The change in the lattice parameters of the ZnO host material depends on the ionic radii of the impurity that substitutes the Zn ions at the lattice sites. In our case, since the ionic radius of Al^{3+} (0.053 nm) used as a dopant is less than that of Zn^{2+} (0.074 nm), Al^{3+} substituting Zn^{2+} will lead to compression of the lattice and hence a decrease in the lattice parameters is observed in Table IV. It is plausible that the increase in temperature provides sufficient energy to thermally activate Zn/Al atoms into the sites in the ZnO film, and this increases the probability of atomic substitution. Site substitutions for atoms with different charge states than host could lead to a reduction in the lattice parameters.[22]

Table IV shows the calculated crystallite sizes for the three peaks with the highest peaks as well as an average size derived using Scherrer's formula shown in the following equation:

$$D_{sh} = \frac{k\lambda}{\beta \cos \theta}, \tag{5}$$

where k is the crystallite shape factor usually 0.9, λ is the X-ray wavelength used which in our case was 1.541 Å, β is the FWHM which is tabulated in Table III while θ is the Bragg's angle in radians.

From Table IV, the average in plane crystallite size becomes larger with increasing annealing temperature in agreement with the results of AFM and SEM analysis. This increase could be attributed to the fact that at high temperature, the atoms have a higher diffusion coefficient and thus can occupy the correct site in the crystal lattice such that the grains with lower surface energy will become larger at high temperature. As a result, the growth orientation develops into one crystallographic direction of the low surface energy, leading to the improvement of the film crystallinity[26]

$$D = D_o e^{\frac{-E_A}{kT}}, \tag{6}$$

where D_o is the diffusion coefficient at reference temperature T.

The dislocation density δ, defined as the length of dislocation lines per unit volume of the crystal (Williamson and Smallman) and the strain present in the thin film were investigated using Eq. (7) and (8), respectively,

$$\delta = \frac{1}{D_{sh}^2}, \tag{7}$$

$$\varepsilon = \frac{\beta \cos \theta}{4}. \tag{8}$$

The strain in the films relaxes with temperature increase as a result of the removal of defects in the lattice or reduction of grain boundary energy at the grain boundary (Table IV). Such a release in strain reduces the variation of interplanar spacing d, leading to the decrease in the dislocation density. The reducing strain and dislocation density together enhance the stoichiometry of the films, which in turn causes the volumetric expansion of thin films and hence improvement of crystallinity.[31]

Figure 9 shows the effect of varied deposition time on the XRD patterns. The films grown at 5 and 10 min are polycrystalline in nature with a preferred orientation along the
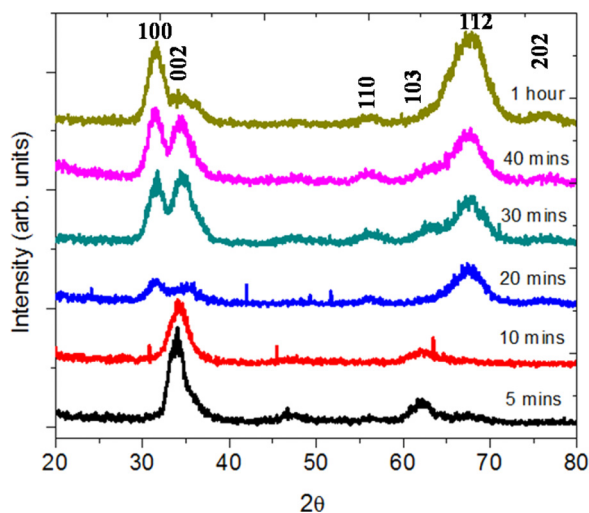
FIG. 9. X-ray diffraction (XRD) pattern of the Al doped ZnO thin film before and after annealing at temperature between 600 and 1000 °C in air.

c-axis, i.e., (002) plane and certain fraction along the (103) plane. Increasing the deposition time shows a decrease in the (002) plane intensity and emergence of the (100) and (112) planes as the preferred orientations. In addition, a shift to higher Bragg's angle is observed. This change in the preferred crystal orientation is attributed to the availability of more Al ions substituting Zn ions as stated in a section earlier in this work.

The surface and interface sensitivity of X-ray reflectivity (XRR) has also been exploited to determine the film density, interfacial roughness, and thickness of Al doped ZnO films. The presence of smooth interfaces is responsible for the Kiessig oscillations in the XRR spectrum for a film deposited for 5 min. Figure 10 represents the simulation of the XRR data in which precise information of the layer thickness, film density, surface, and interfacial roughness has been extracted for the layer.

From the simulation of the specular reflectivity, the thickness and rms roughness of the film deposited at 5 min were found to be 139.49 ± 0.05 nm and 0.51 ± 0.05 nm, respectively. This implies a deposition rate of 278.98 Å/min. The density was found to be 5.56 ± 0.1 gcm^{-3} which is in agreement with the literature value of 5.61 gcm^{-3}. This film

thickness for the film grown for 5 min is in agreement with that obtained from the surface profilometer as shown in Table II. Further measurements of films grown at different deposition times reveal that films deposited on silicon wafer substrates at room temperature show a greater dispersion as the deposition time increases. This is in agreement with the findings of Camacho-Espinosa *et al.*[32] This could also be attributed to variation in the chamber pressure which was not easy to keep constant.

D. PL measurements

Figure 9 shows the room temperature photoluminescence spectra of Al doped ZnO before and after annealing. The spectra were acquired using 229 nm excitation from a frequency-doubled argon ion laser. The spectrometer utilized a 150 lines/mm grating and a 20X UVB objective. The spectrum was acquired from 250 nm to 900 nm at 5 s acquisition time.

The thin films grown at a duration of 40 min without annealing (Fig. 11) show an emission band at 467 nm (2.7 eV). This band is attributed to the near band edge (NBE) emission corresponding to the exciton related transition from the localized level below the conduction band to the valence band. The relatively high wavelength of this band could be as a result of substitution of Zn^{2+} that has a higher ionic radius, 0.074 nm with Al^{3+} of ionic radius 0.053 nm. This confirms the observation made in XRD analysis. Annealing of this film leads to blue-shifting of this peak to around 374.7 nm (3.31 eV) when the annealing temperature is 1000 °C. Several other bands are also formed as shown in Fig. 9. During annealing in air Zn, the interstitials could be reduced or removed since they are shallow donors separating the conduction band and other defect bands leading to a wider optical band gap due to reduced overlapping of the defect band and conduction band.

The band at 439 nm (2.82 eV) emerges when annealing is carried out at 800 °C and increases in intensity with temperature. This could be attributed to O_i centers, which promotes the chemisorption of oxygen hence increasing the density of electronic state in the film.[11] Other bands also emerge upon annealing at 800 °C such as at 488 nm that may be associated to Zn_i^+ and 545 and 600 nm associated with
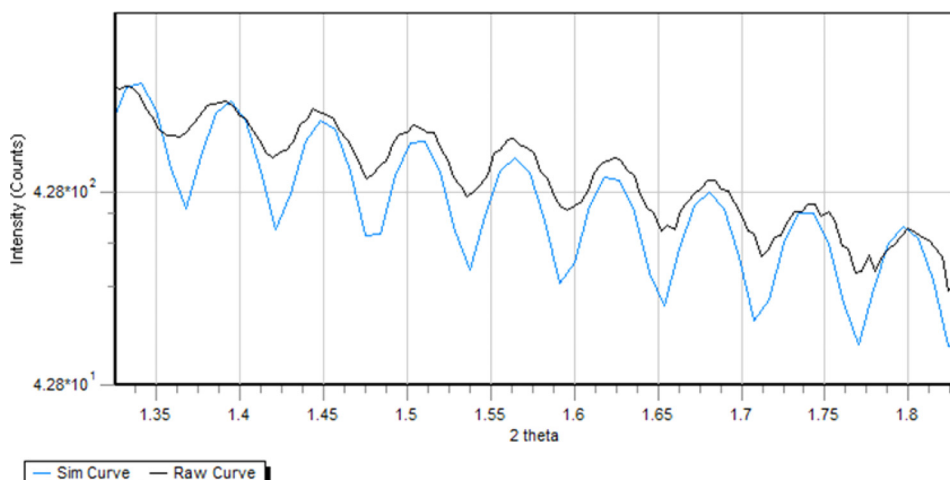

FIG. 10. Experimental (black) and simulated (blue) XRR spectra of the as-deposited Al doped thin film deposited at 100 W for 5 min.
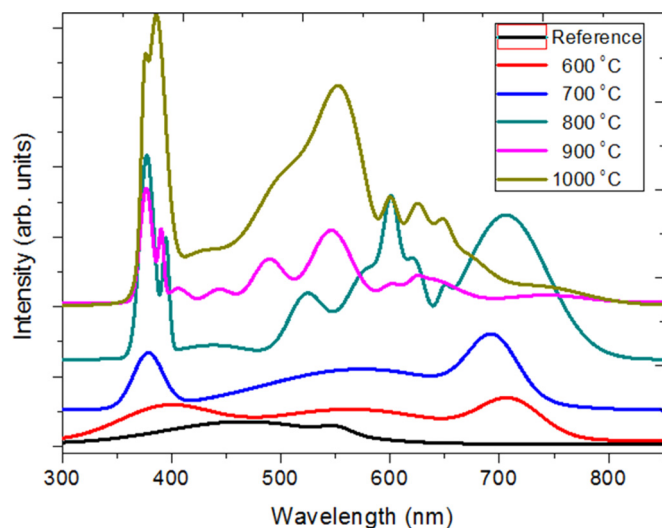
FIG. 11. Room temperature photoluminescence spectra of the Al doped ZnO thin film grown for 40 min before and after annealing at temperature between 600 and 1000 °C in air. The spectra have been stacked for clarity.

$Zn_i^+ \rightarrow V_{Zn}^-$ transition. The band at 523 nm when annealing is carried out at 800 °C increases in intensity with temperature indicating that the concentration of O vacancies increases with temperature.

The thin films grown at a duration of 20 min (Fig. 12) show a blue band near 474 nm (2.62 eV) and a broad shoulder near 720–730 nm. This band (2.62 eV) is attributed to the near band edge (NBE) emission. Increasing the deposition time leads to blue-shifting of this peak to around 421 nm (2.95 eV) when the deposition time is 1 h. The infrared emission at 830.0 nm when the film is grown for 1 h could be attributable to an electronic transition from the Oi 0 to the higher V_{Zn} – level.

IV. CONCLUSION

The influences of thermal annealing and deposition time on the structural and optical features of radio frequency (RF) magnetron sputtered aluminium doped Zinc Oxide on Si (100) are investigated. Preferentially oriented structures of Al doped ZnO along the (100), (002), and (112) directions together with peak shift and reduced strain due to post-annealing between 600 and 1000 °C are established from grazing incidence x-ray diffraction (XRD). Atomic force microscopy (AFM) images showed increasing roughness and particle size. The observed blue-shift and emerging of many photoluminescence peaks resulting from thermal annealing and increase in deposition time have been reported.
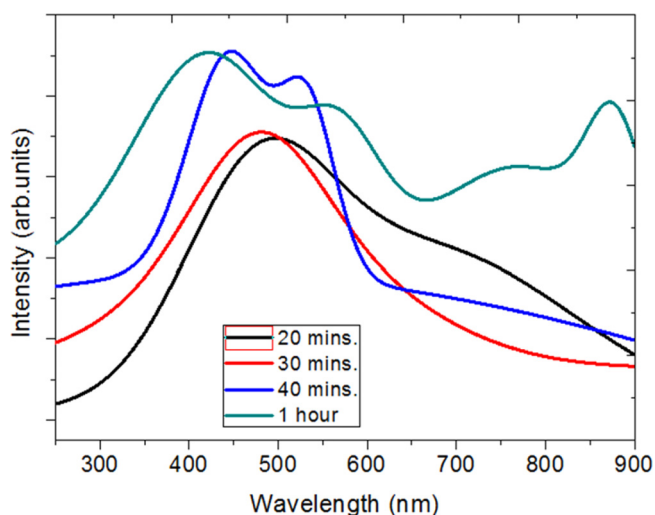
FIG. 12. Room temperature photoluminescence spectra of the Al doped ZnO thin film as-grown at an RF power of 100 W at different deposition times.

[1]G.-S. Kim, S. Ansari, H.-K. Seo, Y.-S. Kim, and H.-S. Shin, "Effect of annealing temperature on structural and bonded states of titanate nanotube films," J. Appl. Phys. **101**, 24314 (2007).

[2]W. M. Yen and H. Yamamoto, *Phosphor Handbook* (CRC Press, 2006).

[3]S. Heinze, A. Krtschil, J. Bläsing, T. Hempel, P. Veit, A. Dadgar, J. Christen, and A. Krost, "Homoepitaxial growth of ZnO by metalorganic vapor phase epitaxy in two-dimensional growth mode," J. Cryst. Growth **308**, 170–175 (2007).

[4]T. Ive, T. Ben-Yaacov, C. Van de Walle, U. Mishra, S. DenBaars, and J. Speck, "Step-flow growth of ZnO (0001) on GaN (0001) by metalorganic chemical vapor epitaxy," J. Cryst. Growth **310**, 3407–3412 (2008).

[5]F. Quaranta, A. Valentini, F. R. Rizzi, and G. Casamassima, "Dual-ion-beam sputter deposition of ZnO films," J. Appl. Phys. **74**, 244–248 (1993).

[6]H. Tian, X. Wang, Y. Zhu, L. Liao, X. Wang, J. Wang, and W. Hu, "High performance top-gated ferroelectric field effect transistors based on two-dimensional ZnO nanosheets," Appl. Phys. Lett. **110**, 043505 (2017).

[7]A. Janotti and C. G. Van de Walle, "Fundamentals of zinc oxide as a semiconductor," Rep. Prog. Phys. **72**, 126501 (2009).

[8]G. W. Tomlins, J. L. Routbort, and T. O. Mason, "Zinc self-diffusion, electrical properties, and defect structure of undoped, single crystal zinc oxide," J. Appl. Phys. **87**, 117–123 (2000).

[9]S. Pandelides, *Deep Centers in Semiconductors: A State-of-the-Art Approach* (Gordon and Breach Science, Yverdon, 1992).

[10]R. K. Willardson, E. R. Weber, and M. Stavola, *Identification of Defects in Semiconductors* (Academic Press, 1998).

[11]S.-Y. Kuo, K.-C. Liu, F.-I. Lai, J.-F. Yang, W.-C. Chen, M.-Y. Hsieh, H.-I. Lin, and W.-T. Lin, "Effects of RF power on the structural, optical and electrical properties of Al-doped zinc oxide films," Microelectron. Rel. **50**, 730–733 (2010).

[12]Z. Fang, Z. Yan, Y. Tan, X. Liu, and Y. Wang, "Influence of post-annealing treatment on the structure properties of ZnO films," Appl. Surf. Sci. **241**, 303–308 (2005).

[13]A. C. S. Sabioni, "About the oxygen diffusion mechanism in ZnO," Solid State Ionics **170**, 145–148 (2004).

[14]A. Janotti and C. G. Van de Walle, "Oxygen vacancies in ZnO," Appl. Phys. Lett. **87**, 122102 (2005).

[15]T. Prasada Rao, M. Santhosh Kumar, and V. Ganesan, "Effect of annealing on the structural, optical and electrical properties of ZnO thin films by spray pyrolysis," Indian J. Phys. **85**, 1381–1391 (2011).

[16]J.-P. Colinge, Silicon, *On-Insulator Technology: Materials to VLSI: Materials to VLSI* (Springer Science & Business Media, 2004).

[17]C-m. Lai, K-m. Lin, and S. Rosmaidah, "Effect of annealing temperature on the quality of Al-doped ZnO thin films prepared by sol–gel method," J. Sol-Gel Sci. Technol. **61**, 249–257 (2012).

[18]Z. Tang, P. C. Chan, R. K. Sharma, G. Yan, I.-M. Hsing, and J. K. Sin, "Investigation and control of microcracks in tin oxide gas sensing thin-films," Sens. Actuators, B **79**, 39–47 (2001).

[19]K. A. Alim, V. A. Fonoberov, M. Shamsa, and A. A. Balandin, "Micro-Raman investigation of optical phonons in ZnO nanocrystals," J. Appl. Phys. **97**, 124313 (2005).

[20]V. Russo, M. Ghidelli, P. Gondoni, C. Casari, and A. L. Bassi, "Multi-wavelength Raman scattering of nanostructured Al-doped zinc oxide," J. Appl. Phys. **115**, 073508 (2014).

[21]M. Tzolov, N. Tzenov, D. Dimova-Malinovska, M. Kalitzova, C. Pizzuto, G. Vitali, G. Zollo, and I. Ivanov, "Vibrational properties and structure of undoped and Al-doped ZnO films deposited by RF magnetron sputtering," Thin Solid Films **379**, 28–36 (2000).

[22]H. ullah, A. Iqbal, M. Zakria, and A. Mahmood, "Structural and spectroscopic analysis of wurtzite $(ZnO)_{1-x}(Sb_2O_3)_x$ composite semiconductor," Prog. Nat. Sci.: Mater. Int. **25**, 131–136 (2015).

[23]O. Lupan, T. Pauporté, L. Chow, B. Viana, F. Pellé, L. Ono, B. R. Cuenya, and H. Heinrich, "Effects of annealing on properties of ZnO thin films prepared by electrochemical deposition in chloride medium," Appl. Surf. Sci. **256**, 1895–1907 (2010).

[24]A. Ismail and M. Abdullah, "The structural and optical properties of ZnO thin films prepared at different RF sputtering power," J. King Saud Univ.-Sci. **25**, 209–215 (2013).

[25]Ü. Özgür, Y. I. Alivov, C. Liu, A. Teke, M. Reshchikov, S. Doğan, V. Avrutin, S.-J. Cho, and H. Morkoç, "A comprehensive review of ZnO materials and devices," J. Appl. Phys. **98**, 041301 (2005).

[26]K. S. Kim, H. W. Kim, and N. H. Kim, "Structural characterization of ZnO films grown on SiO 2 by the RF magnetron sputtering," Phys. B: Condens. Matter **334**, 343–346 (2003).

[27]M. Najafi and H. Haratizadeh, "The effects of Al doping and post-annealing via intrinsic defects on photoluminescence properties of ZnO: Eu nanosheets," Mater. Sci. Semicond. Process. **31**, 76–83 (2015).

[28]T. M. K. Thandavan, S. M. A. Gani, C. San Wong, and R. M. Nor, "Enhanced Photoluminescence and raman properties of Al-Doped ZnO nanostructures prepared using thermal chemical vapor deposition of methanol assisted with heated brass," PloS ONE **10**, e0121756 (2015).

[29]V. Noack and A. Eychmüller, "Annealing of nanometer-sized zinc oxide particles," Chem. Mater. **14**, 1411–1417 (2002).

[30]F. Wang, M. Wu, Y. Wang, Y. Yu, X. Wu, and L. Zhuge, "Influence of thickness and annealing temperature on the electrical, optical and structural properties of AZO thin films," Vacuum **89**, 127–131 (2013).

[31]S. Thanikaikarasan, T. Mahalingam, K. Sundaram, A. Kathalingam, Y. D. Kim, and T. Kim, "Growth and characterization of electrosynthesized iron selenide thin films," Vacuum **83**, 1066–1072 (2009).

[32]E. Camacho-Espinosa, E. Rosendo, T. Díaz, A. Oliva, V. Rejon, and J. Peña, "Effects of temperature and deposition time on the RF-sputtered CdTe films preparation," Superficies Vacío **27**, 15–19 (2014).